Singlet O_2 Reactions with Radical Cations of 8-Bromoguanine and 8-Bromoguanosine: Guided-Ion Beam Mass Spectrometric Measurements and Theoretical Treatments

Jonathan Benny,[a,b] Toru Saito,*[c] May Myat Moe,[a,b] and Jianbo Liu*[a,b]
[a] Department of Chemistry and Biochemistry, Queens College of the City University of New York, 65-30 Kissena Blvd., Queens, NY 11367, USA; [b] Ph.D. Program in Chemistry, the Graduate Center of the City University of New York, 365 5th Ave., New York, NY 10016, USA; and [c] Department of Biomedical Information Science, Graduate School of Information Science, Hiroshima City University, 3-4-1 Ozuka-Higashi, Asa-Minami-Ku, 731-3194 Hiroshima, Japan

Abstract 8-bromoguanosine is generated *in vivo* as a biomarker for early inflammation. Its formation and secondary reactions lead to a variety of biological sequelae at inflammation sites, most of which are mutagenic and linked to cancer. Herein, we report the formation of radical cations of 8-bromoguanine ($8BrG^{\bullet+}$) and 8-bromoguanosine ($8BrGuo^{\bullet+}$) and their reactions toward the lowest excited singlet molecular oxygen ($^1O_2$) — a common reactive oxygen species generated in biological systems. This work aims to investigate synergistic, oxidatively generated damage of 8-brominated guanine and guanosine that may occur upon ionizing radiation, one-electron oxidation and $^1O_2$ oxidation. Capitalizing on measurements of reaction product ions and cross sections of $8BrG^{\bullet+}$ and $8BrGuo^{\bullet+}$ with $^1O_2$ using guided-ion beam tandem mass spectrometry, and augmented by computational modeling of the prototype reaction system, $8BrG^{\bullet+} + {}^1O_2$, using the approximately spin-projected ωB97XD/6-31+G(d,p) density functional theory, the coupled cluster DLPNO-CCSD(T)/aug-cc-pVTZ and the multi-reference CASPT2(21,15)/6-31G**, probable reaction products and potential energy surface (PES) were mapped out. $8BrG^{\bullet+}$ and $8BrGuo^{\bullet+}$ present similar exothermic oxidation products, and their reaction efficiencies with $^1O_2$ increase with decreasing collision energy. Both single-and multi-reference theories predicted that the two most energetically favorable reaction pathways correspond to $^1O_2$-addition to the C8 and C5-positions of $8BrG^{\bullet+}$, respectively. The CASPT2-calculated PES represents the best quantitative agreement with the experimental benchmark in that the oxidation exothermicity is close to the water hydration energy of product ions and, thus, is able to eliminate a water ligand in the product ions.

* Corresponding author: Jianbo Liu, e-mail: jianbo.liu@qc.cuny.edu. Tel: 1-718-997-3271.
Co-corresponding author: Toru Saito, e-mail: tsaito@hiroshima-cu.ac.jp.

1. Introduction

Human leukocyte enzymes myeloperoxidase (MPO) and eosinophil peroxidase (EPO), which are released in association with helminthic infections and various inflammatory disease processes, can selectively catalyze the reaction of bromide (at a physiological plasma [Br^-] = 20 – 100 μM)[1] with hydrogen peroxide to form hypobromous acid (HOBr) and hypobromite ion (OBr^-) *in vivo*.[1-3] Besides oxidizing the cellular materials of invading pathogens, excess HOBr and OBr^- may brominate host DNA, proteins and lipids.[4-5] Guanine is the preferred purine target for bromination as a free nucleobase, while adenine is the major target for bromination in double stranded DNA.[4] Stable brominated DNA adducts include 8-bromo-2′-deoxyguanosine, 8-bromo-2′-deoxyadenosine and 5-bromo-2′-deoxycytidine.[4, 6] Notably, 8-bromo-2′-deoxyguanosine was observed prior to 8-oxo-2′-deoxyguanosine (abbreviated as OG, the most commonly used biomarker for oxidatively generated DNA damage)[7] with respect to the order of guanine modifications, suggesting that 8-bromo-2′-deoxyguanosine is a biomarker for early inflammation.[8] Moreover, only 8-bromo-2′-deoxyguanosine, not 8-bromo-2′-deoxyadenosine nor 5-bromo-2′-deoxycytidine, is a mutagenic lesion.[9] 8-bromo-2′-deoxyguanosine contributes to mutagenic and cytotoxic events at inflammation sites, such as the formation of a Hoogsteen base pair with guanine,[10] the promotion of one-base deletion, and the misincorporation of guanine, adenine and thymine nucleobases opposite the 8-bromo-2′-deoxyguanosine lesion in human cells.[9-10] All of the aforementioned provide an important link between the formation of 8-bromo-2′-deoxyguanosine and cancer. On the other hand, brominated nucleotides are considered potential radiosensitizers[11] that form radicals to enhance cytotoxic DNA lesions[12-14] and promote strand breaks[15-16] by the given dose of ionizing radiation in radiotherapy for cancer treatment. In the context of radiosensitivity of brominated nucleosides, most research focused on the formation of their radical anions and derivatives via electron attachment.[12-16] To the best of our knowledge, few studies were carried out concerning the formation of radical cations of brominated nucleosides.

An important criterion that determines the tendency of a nucleobase/nucleoside to form a radical

cation is adiabatic ionization energy (AIE), which is 7.75 eV for guanine,[17-18] 8.267 eV for adenine,[18-19] 8.66 eV for cytosine[18-19] and 8.82 eV for thymine.[18, 20] It indicates guanine as the primary target for one-electron oxidation among the four normal DNA nucleobases. No experimental AIE is available for the 8-bromoguanine nucleobase or nucleoside. According to the ωB97XD/6-31+G(d,p) prediction, the AIE of 8-bromoguanine is only 0.01 eV higher than that of guanine. This implies that, should the 8-bromoguanine nucleobase and nucleoside form in biological systems, the formation of their radical cations is as facile as those of guanine and guanosine.

The present work focuses on reactions of the radical cations of 8-bromoguanine (abbreviated as $8BrG^{\bullet+}$) and 8-bromoguanosine ($8BrGuo^{\bullet+}$) with electronically excited singlet oxygen O_2 [$a^1\Delta_g$].[21-22] $^1O_2$ is a biologically relevant reactive oxygen species that reacts efficiently with celluar constituents including proteins, DNA and lipids.[23] Guanine represents the exclusive DNA target for $^1O_2$.[24-41] The resulting primary and secondary damage of guanine nucleobases and nucleosides is implicated in DNA strand breaks,[42] DNA-protein cross-links,[34, 39] mutation[43] and apoptosis[44] as well as in photodynamic therapy for cancer.[45] Interestingly, oxidized forms of guanine such as OG are even more susceptible to the $^1O_2$ oxidation than guanine and guanosine.[26, 46-56] However, no study has been reported for the $^1O_2$ oxidation of neutral 8BrG, 8BrGuo or their radical cations. Capitalizing on the formation of $8BrG^{\bullet+}$ and $8BrGuo^{\bullet+}$ in the gas phase and the measurements of their reactions with $^1O_2$ using a guided-ion beam tandem mass spectrometer, and augmented by theoretical modeling at single- and multi-reference levels, we were able to delineate their reaction mechanisms, pathways and product structures, and compare the oxidizability of $8BrG^{\bullet+}$ with the unsubstituted guanine radical cation.

2. Experimental and Theoretical Methods

2.1 Chemicals, instrumentation, and experimental procedures

8BrG (Biosynth, 97%), 8BrGuo (TCI, 98%), $Cu(NO_3)_2$ (Alfa Aesar, 99.999%), KOH (Fisher Chemical, >85%), 2′-deoxyguanosine (dGuo, MilliporeSigma, > 99%) and H_2O_2 (Acros Organics, 35 wt%) were used as received from commercial sources. The Cl_2 gas (99.5%) was purchased from Sigma-

Aldrich. The He gas (research grade) was purchased from T.W. Smith. All solvents were HPLC grade.

$^1O_2$ was produced by the reaction of $H_2O_2 + Cl_2 + 2KOH \rightarrow O_2(a^1\Delta_g)/O_2(X^3\Sigma_g) + 2KCl + 2H_2O$, wherein both $O_2(a^1\Delta_g)$ and $O_2(X^3\Sigma_g)$ were produced.[57] The experimental setup for $^1O_2$ generation and detection was reported previously.[58-59] In brief, 10.5 ml of 8 M KOH was slowly added to 20 mL of 35 wt% H_2O_2 in a sparger at -19°C. The cold mixture was then degassed. 3.42 sccm of the Cl_2 gas and 53.5 sccm of the He gas were mixed in a gas proportioner and bubbled through the H_2O_2/KOH slush. The reaction quantitatively converted Cl_2 into a mixture of $O_2(a^1\Delta_g)/O_2(X^3\Sigma_g)$ and produced the O_2 gas at the same flow rate as that of the Cl_2 input. The gas product passed through a cold trap at -70 °C to remove water vapor and was thereupon comprised of only $O_2(a^1\Delta_g)/O_2(X^3\Sigma_g)$ and He. The gas products subsequently flew through an emission cell, where the phosphorescence from the $O_2(a^1\Delta_g, \nu' = 0) \rightarrow O_2(X^3\Sigma_g, \nu = 0)$ transition at 1270 nm passed through an optical chopper and a 1270 nm-centered interference filter and was focused into a cooled InGaAs detector coupled with a lock-in amplifier. Emission intensities were converted to absolute $^1O_2$ concentrations on the basis of a previous calibration.[59] To reduce wall- and self-quenching of $^1O_2$, the sparger was continuously evacuated and its pressure was maintained at 12.8 Torr. At this pressure, the concentration of $^1O_2$ in the gas product was steadily maintained at 15% during the experiment.

Ion-molecule reactions of $8BrG^{\bullet+}$ and $8BrGuo^{\bullet+}$ with $^1O_2$ were carried out on a home-built guided-ion beam tandem mass spectrometer coupled with an electrospray ionization (ESI) ion source.[60] Radical cations of $8BrG^{\bullet+}$ and $8BrGuo^{\bullet+}$ were produced by collision-induced dissociation (CID) of copper(II)-nucleobase/nucleoside complexes, following an approach which was first developed by Siu *et al.* for the formation of oligopeptide radical cations in the gas phase[61] and later applied to the formation of nucleobase/nucleoside radical cations by the O′Hair group[62] and Bohme group.[63] In the present experiment, a methanol/water (v:v = 2:1) solution containing of 0.25 mM 8BrG, 0.25 mM dGuo and 0.25 mM $Cu(NO_3)_2$ was freshly made and sprayed to the air through an ESI needle at a flow rate of 0.06 mL/h. The ESI needle was biased at 2.4 kV with respect to ground, the Cu^{II}-8BrG-dGuo complexes (wherein

dGuo was used as a co-ligand to enhance complex formation)[41] formed in the electrospray entered the source chamber of the mass spectrometer through a desolvation capillary which was biased at 225 V with respect to ground and heated to 181 °C. A 1.0-mm skimmer is located 3 mm away from the end of the capillary, separating the source chamber and a radio-frequency (rf) hexapole ion guide. The skimmer was biased at 18 V with respect to ground. The electrical field between the capillary and the skimmer prompted the CID of the Cu^{II}-8BrG-dGuo complexes. Among the complexes, $[Cu^{II}(8BrG)_{3-n}(dGuo)_n]^{\bullet 2+}$ underwent redox separation and formed $[Cu^{I}(8BrG)_{2-n}(dGuo)_n]^{+}$ + $8BrG^{\bullet +}$ and $[Cu^{I}(8BrG)_{3-n}(dGuo)_{n-1}]^{+}$ + $dGuo^{\bullet +}$. Under mild heating condition, monohydrated radical cations were generated as well. The ion-beam intensities were 1.2×10^5 counts/s for $8BrG^{\bullet +}$ and 5×10^4 counts/s for its monohydrate. $8BrGuo^{\bullet +}$ was produced in a similar way, by electrospray of a mixture of 0.25 mM 8BrGuo, 0.25 mM dGuo and 0.25 mM $Cu(NO3)_2$ in 2:1 methanol/water. The ion-beam intensity of $8BrGuo^{\bullet +}$ was 7×10^4 counts/s.

Radical cations were transported to the hexapole ion guide, where they underwent energy damping via collisions with the background gas (at a pressure of 20 mTorr) and therefore were thermalized to room temperature and focused in the radial direction. Ions were then mass selected by a quadrupole mass filter and injected into an octopole ion guide that passes a scattering cell containing the $^1O_2$ target gas. The octopole ion guide was driven by a combination of rf potential and DC bias. The rf potential was used to trap ions in the radial direction while the DC bias was used to control the kinetic energy of reactant ions in the lab frame (E_{lab}). The center-of-mass collision energy (E_{col}) for ion-molecule reactions was set by $E_{col} = E_{lab} \times m_{neutral}/(m_{neutral} + m_{ion})$ where $m_{neutral}$ and m_{ion} are the masses of the neutral and ionic reactants, respectively. After ion-molecule scattering, product ions and remaining reactant ions were collected by the octopole and guided into a second quadrupole mass filter for mass analysis. Ion signals were registered using a pulse-counting electron multiplier.

The gas pressure (including $^1O_2$, $^3O_2$ and He) within the scattering cell was maintained at 0.25 mTorr, where radical cations had at most single collisions with O_2 molecules. Under the single ion-molecule collision conditions, reaction cross sections were calculated from the ratio of reactant/product ion

intensities, the pressure and concentration of $^1O_2$ within the scattering cell, and the effective cell length for collisions. To verify that 8BrG$^{\bullet+}$ and 8BrGuo$^{\bullet+}$ were not reactive toward $^3O_2$, control experiments were carried out under the same conditions except that the mixture of pure $^3O_2$ and He was used as the target gas for ion-molecule collisions. No reaction was observed except the CID of 8BrG$^{\bullet+}$ and 8BrGuo$^{\bullet+}$.

2.2 Electronic structure calculations

DFT calculations Geometries of reactants, intermediate complexes, transition states (TSs) and products were fully optimized using the density functional theory (DFT) ωB97XD/6-31+G(d,p). This range-separated functional mitigated self-interaction errors and improved orbital description of radical cations.[64] All TSs were verified to have only one imaginary frequency which corresponds to the anticipated reaction pathway. Intrinsic reaction coordinate (IRC) calculations were carried out to verify that each TS was connected to the correct react/product minima. DFT calculations were performed using Gaussian 16.[65] Atomic charge populations were analyzed using NBO 6.0.[66]

One challenge in the DFT calculations concerns the multiconfigurational $^1O_2$ wave function that mixes open- and closed-shell characters.[67] The spin-restricted DFT is incapable of treating static correlation arising from the two degenerate π* antibonding orbitals and overestimates the $^1O_2$ excitation energy; while the broken-symmetry, spin-unrestricted DFT brings about spin contamination from $^3O_2$. The problem exists in both the $^1O_2$ reactant and $^1O_2$-adducts. The situation becomes more complicated in reactions of $^1O_2$ with doublet-state radical cations, which leads to two doublet states and one quartet state in products. To assess spin contamination in reaction potential energy surface (PES), all ωB97XD/6-31+G(d,p)-optimized reaction structures were subjected to a T1 diagnostic[68-69] at the DLPNO-CCSD(T)/ aug-cc-pVTZ level of theory[70] using ORCA 4.2.[71] The inclusion of a perturbative correction for triple excitation in CCSD(T) compensated for the deficiencies of a single-determinant reference to some extent. Therefore, CCSD(T) has the capability of handling modest spin contamination.

Approximate spin projection The electronic structure of $^1O_2$ computed with broken-symmetry DFT is

inherently an equal mixture of singlet $^1O_2$ (↑↓, S = 0) and triplet $^3O_2$ (↑↑, S = 0). Previous computational studies revealed that the effect of spin contamination from the triplet state causes an error of more than 0.4 eV in the energy of $^1O_2$.[72-74] It can be anticipated that spin contamination would affect the reaction PES of $^1O_2$ with the radical cation of 8BrG$^{\bullet+}$ (↑, S = $\frac{1}{2}$). Specifically, the target doublet state ^{2}[$^1O_2$ (↑↓) ••• 8BrG$^{\bullet+}$ (↑)] in a reactant precursor complex may suffer from an energetically lower-lying quartet state ^{4}[$^3O_2$ (↑↑) ••• 8BrG$^{\bullet+}$ (↑)]. We used Yamaguchi′s approximate spin projection scheme[75] to remove the spin contamination for reactants, intermediates, TSs, and products. The spin-projected energy is given by

$$E = \frac{\langle \hat{\mathbf{S}}^2 \rangle^{\mathrm{HS}} - \langle \hat{\mathbf{S}}^2 \rangle^{\mathrm{BS}}_{\mathrm{exact}}}{\langle \hat{\mathbf{S}}^2 \rangle^{\mathrm{HS}} - \langle \hat{\mathbf{S}}^2 \rangle^{\mathrm{BS}}} E^{\mathrm{BS}} - \frac{\langle \hat{\mathbf{S}}^2 \rangle^{\mathrm{BS}} - \langle \hat{\mathbf{S}}^2 \rangle^{\mathrm{BS}}_{\mathrm{exact}}}{\langle \hat{\mathbf{S}}^2 \rangle^{\mathrm{HS}} - \langle \hat{\mathbf{S}}^2 \rangle^{\mathrm{BS}}} E^{\mathrm{HS}} \quad (1)$$

where E^{BS} and $\langle \hat{\mathbf{S}}^2 \rangle^{\mathrm{BS}}$ represent the computed total energy and the expectation value of the total spin angular momentum operator for a target broken-symmetry state; E^{HS} and $\langle \hat{\mathbf{S}}^2 \rangle^{\mathrm{HS}}$ are the counterparts for the corresponding high-spin state. When the influence of spin contamination is negligible, the $\langle \hat{\mathbf{S}}^2 \rangle^{\mathrm{BS}}$ value for a spin-contaminated solution is close to its exact value ($\langle \hat{\mathbf{S}}^2 \rangle^{\mathrm{BS}}_{\mathrm{exact}}$) defined as

$$\langle \hat{\mathbf{S}}^2 \rangle^{\mathrm{BS}}_{\mathrm{exact}} = \frac{N^\alpha - N^\beta}{2}\left(\frac{N^\alpha - N^\beta}{2} + 1\right) \quad (2)$$

where N^α and N^β are the number of alpha and beta electrons. The BS and HS states were set to singlet and triplet for the $^1O_2$ reactant, and doublet and quartet for the remaining species, respectively. Note that a direct sum of the pre-computed molecular orbitals for $^1O_2$ (↑↓) and 8BrG$^{\bullet+}$ (↑) was used as an initial guess to compute the reactant precursor complex in the correct doublet state ^{2}[$^1O_2$ (↑↓) ••• 8BrG$^{\bullet+}$ (↑)]. Otherwise, a lower-energy but incorrect doublet state ^{2}[$^3O_2$ (↑↑) ••• 8BrG$^{\bullet+}$ (↓)] was obtained.

CASPT2 Energies of the DFT optimized reaction structure were recalculated using the multi-reference active space self-consistent field method CASPT2/6-31G**,[76-77] which adds dynamical correlation to the CASSCF[78] wave function using the second order perturbation theory. The size of the active space is (9, 7) for 8BrG$^{\bullet+}$, (12, 8) for $^1O_2$, and (21, 15) for the reaction structures. The active spaces include the $\sigma_{O(2p)-O(2p)}$, $\sigma^*_{O(2p)-O(2p)}$, $\sigma_{O(2\pi)-O(2\pi)}$, $\pi_{\pm1}$, $\pi^*_{\pm1}$ and $\sigma^*_{O(2\pi)-O(2\pi)}$ orbitals in O_2, and the π orbitals in 8BrG$^{\bullet+}$ that have participated in and/or affected the formation of $^1O_2$-adducts. Reaction enthalpy reported at the

CASPT2/6-31G** level of theory is based on the sum of the CASPT2-calculated electronic energy and the 298 K thermal correction calculated at ωB97XD/6-31+G(d,p) (including ZPE which was scaled by factor of 0.975).[79] The CASPT2 calculations were carried out using OpenMolcas ver. 21.06,[80-81] and the shift parameter for ionization potential-electron affinity (IPEA) was set to 0.25 a.u..[82]

3. Results and Discussion

3.1 Gas-phase structures of 8BrG$^{\bullet+}$ and 8BrGuo$^{\bullet+}$

The neutral 8BrG has various tautomers namely keto_N9H, enol_N9H, keto_N7H and enol_N7H. The keto forms are appreciably more stable than the corresponding enol forms in the gas phase, and the keto_N7H form is more stable than the keto_N9H form.[83] We compared the energies of these tautomers at their cation states using the ωB97XD/6-31+G(d,p) method, and included two rotamers (*syn*- and *anti*- with respect to the imidazole ring) for each of the enol_N9H and enol_N7H structures. As depicted in Scheme S1 in the Supporting Information, in contrast to their neutral molecular counterparts, the keto_N9H cation overwhelmingly dominates in the gas phase with a thermal population of > 97% at room temperature. This structure was therefore used as the reactant structure in data analysis and computations.

Scheme 1 compares the spin and charge distributions of 8BrG$^{\bullet+}$ and 8BrGuo$^{\bullet+}$ in their keto_N9H forms. The two species share the same spin density and atomic charge distributions, with the unpaired electron delocalized over the C2, N3, C4, C5, O6, N7, C8 and Br atoms and the charge centered on the C4 and C5 atoms in both systems. Therefore, it is reasonable to expect that the chemistry of 8BrG$^{\bullet+}$ and 8BrGuo$^{\bullet+}$ should be alike.

3.2 Reaction products and cross sections for $^1O_2$ with 8BrG$^{\bullet+}$ and 8BrGuo$^{\bullet+}$.

A common feature of the $^1O_2$ reactions with guanine nucleobase ions[35-36, 40] and their derivatives[41, 56] is that the reaction is exothermic and has no activation barriers above starting reactants. As a result, in a rarefied gas-phase reaction, heat release is deposited into product internal modes (mostly vibrational modes) and causes the decomposition of vibrationally excited product ions into starting reactants in a short time scale. This scenario was also observed in the reaction of $^1O_2$ with 8BrG$^{\bullet+}$, wherein no

oxidation product ions survived the ion time-of-flight (~10^2 μs) within our mass spectrometer. To prevent this unfavorable decomposition and capture $^1O_2$-oxidation product ions in the mass spectrometer, our strategy is to use hydrated reactant ions.[35-36, 40-41, 56] In that case, the reaction heat of formation, which would otherwise prompt decomposition of the nascent O_2-adduct, is mostly consumed for a water ligand elimination and accompanying kinetic energy release.

Following this idea, ion-molecule collisions of monohydrated 8BrG$^{\bullet+}$·H_2O with $^1O_2$ were examined. Scheme 2 presents various structures of 8BrG$^{\bullet+}$·H_2O, of which 8BrG$^{\bullet+}$·W12b has the water ligand hydrogen-bonded to N1-H and N2-H with hydration energy of -0.78 eV and a population of 97% and thus represents the most probable monohydrated reaction ion structure. Figure 1a shows a product ion mass spectrum for the reaction of 8BrG$^{\bullet+}$·H_2O (*m/z* 247 for the ^{79}Br-only reactant ion) + $^1O_2$ recorded at E_{col} = 0.05 eV as well as reaction cross section measured as a function of E_{col} over the range of 0.05 to 0.5 eV. Product ions were detected at *m/z* = 261, which corresponds to the liberation of a water ligand from a [8BrG$^{\bullet+}$·H_2O + O_2] adduct. The reaction is exothermic and has no activation barrier above the reactants, as we can judge on the basis of the exothermic type E_{col}-dependence of the reaction. The measurement also indicates that the energy release from the $^1O_2$ oxidation of 8BrG$^{\bullet+}$ must be larger than the elimination energy of a water ligand in the product ion. Only under this condition can the reaction system liberate a water ligand barrierlessly following the $^1O_2$ addition. The experimental finding that the oxidation reaction enthalpy is no less than the water elimination energy was used as a benchmark to test different computational methods utilized in PES calculations.

Due to the low ion beam intensity of monohydrated 8BrGuo$^{\bullet+}$·H_2O, we were not able to collect their oxidation product ions. But we managed to detect a small fraction of oxidation product ions from the reaction of dry 8BrGuo$^{\bullet+}$ (*m/z* 361 for the ^{79}Br-only reactant ions) with $^1O_2$, as shown in Figure 1b. The successful capture of the exothermic product ions of dry 8BrGuo$^{\bullet+}$ is presumable because the large molecular size of guanosine enhanced intramolecular vibration redistribution (IVR) of reaction heat of formation and slowed down complex decomposition, so that a fraction of the [8BrGuo$^{\bullet+}$-O_2] adduct (*m/z*

393, as shown in Figure 1b) survived the ion time-of-flight and were detected.

Reaction cross sections for both $8BrG^{\bullet+}\cdot H_2O$ and $8BrGuo^{\bullet+}$ increase with decreasing collision energy. The reaction efficiency for $8BrG^{\bullet+}\cdot H_2O$, estimated as $\sigma_{reaction}/\sigma_{collision}$ (where $\sigma_{collision}$ represents the ion-induced dipole capture cross section[84]), is up to 9.5% at E_{col} = 0.05 eV, decreasing to 3% at 0.4 eV and becoming negligible at E_{col} above 0.5 eV. Due to the aforementioned reason, the efficiency for $8BrGuo^{\bullet+}$ is much lower compared to that for $8BrG^{\bullet+}\cdot H_2O$, with the maximum efficiency being 0.15% at the lowest E_{col}. Therefore, the experimental measurement of $8BrGuo^{\bullet+}$ serves only as a qualitative diagnostic to confirm that $8BrGuo^{\bullet+}$ presents a similar reaction product and thermodynamics as those of $8BrG^{\bullet+}$.

3.3 Overview of $^1O_2$-addition pathways and products.

In view of the similar $^1O_2$-oxidation outcomes of $8BrG^{\bullet+}$ and $8BrGuo^{\bullet}$, $8BrG^{\bullet+}$ was used as a prototype to map out oxidation product structures and PES. The ChemDraw structures in Scheme 3 present reaction intermediates, TSs and products optimized at ωB97XD/6-31+G(d,p), all of which are initialized by the formation of a precursor complex bounded by the electrostatic interaction between $8BrG^{\bullet+}$ and $^1O_2$. Their Cartesian coordinates are provided in the Supporting Information. The ωB97XD calculations have proposed four different O_2-addition pathways following the formation of the precursor.

The first addition pathway represents a 5,8-concerted cycloaddition of O_2 via the transition state TS58, leading to the formation of $[5,8\text{-OO-}8BrG]^{\bullet+}$. In $[5,8\text{-OO-}8BrG]^{\bullet+}$, the unpaired electron is located on the imidazole ring, whereas the positive charge shifts to the 6-membered ring. The second addition pathway can be characterized as C8-terminal O_2-addition. There are two possible routes which lead to the same $[8\text{-OO-}8BrG]^{\bullet+}$ product ions, but with a *syn*- and *anti*-configuration, respectively, with respect to the imidazole ring. The *syn*- and *anti*-$[8\text{-OO-}8BrG]^{\bullet+}$ can interconvert between each other via TS8b. The *syn*-$[8\text{-OO-}8BrG]^{\bullet+}$ may interconvert to $[5,8\text{-OO-}8BrG]^{\bullet+}$ via TS8d, which accounts for an alternative, stepwise mechanism for the cycloaddition.

The last two pathways correspond to C4- and C5-terminal additions, respectively. The two pathways adopt a similar pattern, producing *syn*- and *anti*-$[4\text{-OO-}8BrG]^{\bullet+}$ and *syn*- and *anti*-$[5\text{-OO-}8BrG]^{\bullet+}$,

respectively. The [4-OO-8BrG]$^{\bullet+}$ may isomerize to [5-OO-8BrG]$^{\bullet+}$ via TS4d. In all of the 4, 5, and 8-peroxides, the spin is centered on the O_2 moiety; on the other hand, the charge of [8-OO-8BrG]$^{\bullet+}$ is localized on the 6-membered ring, whereas the charges of [4-OO-8BrG]$^{\bullet+}$ and [5-OO-8BrG]$^{\bullet+}$ are localized on the imidazole ring.

The ωB97XD/6-31+G(d,p)-calculated reaction enthalpies for various reaction pathways are listed in Table 1. Included in the table are the values of $<S^2>$ calculated before and after the annihilation of spin contamination in wavefunctions. Theoretically, the value of $<S^2>$ is 0.000 for a pure singlet state and 0.750 for a pure doublet state. According to the spin values, only the $^1O_2$ and the precursor complex present severe spin contamination.

3.4 T1 Diagnostic and reaction PES evaluated at DLPNO-CCSD(T)

A more reliable test for spin contamination was performed using the coupled cluster theory T1 diagnostic of Lee and Taylor,[68-69] wherein $T_1 = \|t_1\|/\sqrt{n}$ (*i.e.*, the Frobenius norm of the single-excitation amplitude vector divided by the square root of the number of electrons correlated). Empirically, a T_1 value that is greater than 0.02 for a closed-shell system or greater than 0.03 for an open-shell system indicates severe multiconfigurational characters or nondynamical correlation effects.

Table 1 includes the results for $<S^2>$ and T_1 diagnostic as well as the single-point reaction energies calculated at DLPNO-CCSD(T)/aug-cc-pVTZ//ωB97XD/6-31+G(d,p). For most reaction structures, the $<S^2>$ value evaluated at the DLPNO-CCSD(T) level matches that calculated after annihilation at the ωB97XD/6-31+G(d,p) level. At both levels, the $<S^2>$ for the precursor complex is deemed the most problematic. According to the T_1 diagnostic, the precursor, TS58 and TS8d have T_1 exceeding 0.02. The DLPNO-CCSD(T)-predicted reaction PES is plotted in Figure 2a. Comparing the reaction energies calculated at DLPNO-CCSD(T)/aug-cc-PVTZ *vs*. those at ωB97XD/6-31+G(d,p), the largest deviation was observed for the precursor, for which the DLPNO-CCSD(T) energy was 1.22 eV higher than the ωB97XD energy. For the other reaction species, differences between the energies at the two levels of theory range from 0.10 to 0.23 eV. The PES indicates that, among the four different O_2-addition

pathways, C8-addition is energetically most favorable, followed by the C5- and then the C4-addition. The 5,8-cycloaddition is the most energy demanding, regardless of being concerted or stepwise.

3.5 Reaction energies refined using approximate spin projection

As aforementioned, the major discrepancy between the DLPNO-CCSD(T)/aug-cc-pVTZ and ωB97XD/6-31+G(d,p) calculations concerns that the ωB97XD energy of the precursor appears to be suspiciously low. As demonstrated by the spin configurations in Scheme 4, the DFT calculation without using a suitable initial guess produced a lower-energy doublet state for the precursor (-1.79 eV with respect to the separated $8BrG^{\bullet+}$ + $^1O_2$) by combining $8BrG^{\bullet+}$ (↓, S = $\frac{1}{2}$ and $m_S = -\frac{1}{2}$) with $^3O_2$ (↑↑, S = 1) but not with $^1O_2$ (↑↓, S = 0). This state is energetically close to the quartet state (-1. 77 eV) that consists of $8BrG^{\bullet+}$ (↑, S = $\frac{1}{2}$ and $m_S = +\frac{1}{2}$) and $^3O_2$ (↑↑, S = 1). The use of a good initial guess gave the higher-lying target doublet state that correctly combines $8BrG^{\bullet+}$ (↑, S = $\frac{1}{2}$ and $m_S = +\frac{1}{2}$) and $^1O_2$ (↑↓, S = 0), with a relative enthalpy of -0.58 eV after the approximate spin projection correction.

As a general observation, the restricted ωB97XD overestimated reaction exothermicity due to the lack of static correlation, while the broken symmetry BS-uωB97XD predicted all reactions as being endothermic (due to large spin contamination). It is mostly related to the energy calculations of the $^1O_2$ reactant and the precursor complex. To obtain accurate PES, the Yamaguchi′s approximate spin projection[72-74] was adopted to correct for spin contamination in $^1O_2$ and in the precursor complex. Note that the late-stage complexes and TSs are dominated by single electronic states, thus spin contamination is no longer a serious issue.

Figure 2b reports the spin-projected ωB97XD/6-31+G(d,p) PES, and the corresponding reaction energies are appended to Table 1. The spin-projected PES lies approximately 0.5 eV higher in energy than that calculated at the DLPNO-CCSD(T) level. Consequently, the spin-projected DFT calculations predict that the C5- and C8-addition pathways are exothermic, whereas the C4-addition and 5,8-cycloaddition are endothermic by ~0.3 eV.

The major discrepancy between the spin-projected DFT calculation results and the ion-beam experiment is that, according to the spin-projected reaction PES, no product channel has reaction heat of formation high enough to overcome the water hydration energy (in the range of -0.78 to -0.8 eV, as shown in Scheme 2) of the corresponding product ions. This implies that the approximate spin projection has not sufficiently corrected for spin contaminations. Otherwise, no water-eliminated oxidation product ions would have been detected in the experiment.

3.6 Multiconfigurational PES assessed at CASPT2 and Comparison with Experimental Benchmark

The CASSCF theory[78, 85] is another approach for treating multi-configuration reaction PESs. However, CASSCF includes primarily nondynamical electron correlation and thus electron correlation energy is treated in an unbalanced way, only that corresponding to active orbitals (*i.e.*, static correlation) is considered. As a result, CASSCF tends to significantly increase reaction activation barriers and product energies as we observed in the CASSCF-calculated reaction PESs for $^1O_2$ with neutral guanine,[34] $9MG^{\bullet+}$ [40] and $9MOG^{\bullet+}$ (radical cation of 9-methyl-8-oxoguanine).[41] As a workaround to this problem, we adopted the CASPT2 method which includes second-order perturbation theory in CASSCF to correct for dynamical correlation. A composite CASPT2/DFT approach (*i.e.*, single-point CASPT2 energy calculations of DFT-optimized geometries) was able to produce correct PESs for the $^1O_2$ reactions with neutral alkenes,[67] 1,3-cyclohexadiene,[34, 86] neutral guanine and histidine,[87] and $9MG^{\bullet+}$ and $9MOG^{\bullet+}$.[40-41]

Figure 2c presents the CASPT2-calculated reaction PES. Their energy values are listed in Table 1 as well. For most reaction species, the CASPT2 energy is 0.3 – 0.5 eV higher than the DLPNO-CCSD(T) energy but 0.2 – 0.4 eV lower than the spin-projected ωB97XD energy. The exception is the precursor complex, for which the CASPT2 energy is 0.65 eV lower than both DLPNO-CCSD(T) and spin-projected ωB97XD-calculated values. On the basis of the CASPT2 PES, the most probable product channel corresponds to reactants → precursor → TS8c (ΔH = -0.84 eV)→ *syn*-$[8\text{-OO-8BrG}]^{\bullet+}$ (ΔH = -0.79 eV), followed by reactants → precursor → TS8a (-0.68 eV)→ *anti*-$[8\text{-OO-8BrG}]^{\bullet+}$ (-0.75 eV) and reactants → precursor → TS5a (-0.75 eV)→ *anti*-$[5\text{-OO-8BrG}]^{\bullet+}$ (ΔH = -0.73 eV). The hydration energy for *syn*-/

a*nti*-[8-OO-8BrG]$^{\bullet+}$ and *anti*-[5-OO-8BrG]$^{\bullet+}$ are all -0.8 eV (see Scheme 2). Therefore, the CASPT2-calculated exothermicity for each of the three probable product ions, combined with the thermal energies (0.2 eV) of the reactants, is sufficient to eliminate a water ligand in the *syn*-/*anti*-[8-OO-8BrG]$^{\bullet+}\cdot H_2O$ or *anti*-[5-OO-8BrG]$^{\bullet+}\cdot H_2O$ product. The CASPT2 PES is thus consistent with the experimental benchmark, rendering itself the most reliable theory for treating the present reaction system.

3.7 Effects of the C8-Br substitution revealed by comparison with the $^1O_2$ oxidation of G$^{\bullet+}$

Qualitatively, 8BrG$^{\bullet+}$ and the unsubstituted G$^{\bullet+}$ [40-41] present the same reaction mechanism toward $^1O_2$. In both cases, the C8-addition presents the energetically most favorable pathway, followed by the C5- and then the C4-addition. In both cases, a cycloaddition to form an endoperoxide is neither kinetically favorable nor energetically feasible at low energies. This is opposite to the $^1O_2$ reactions with closed-shell, neutral guanine molecule[24] or its protonated ions,[35-36] wherein the cycloaddition dominates.

Quantitatively, the reaction efficiency of 8BrG$^{\bullet+}$ with $^1O_2$ is 9.5% at E_{col} = 0.05 eV, decreasing to 3% at 0.4 eV. For comparison, the efficiency of G$^{\bullet+}$ with $^1O_2$ is only 2% at E_{col} = 0.05 eV, decreasing to 1.4% at 0.1 eV. Therefore, the reactivity of 8BrG$^{\bullet+}$ is 5-fold higher than that of the unsubstituted G$^{\bullet+}$. This enhanced reactivity may be interpreted in terms of electronic structures and reaction energetics: first, there exist conjugative interactions between the two $2\pi_{\pm}$ orbitals of O_2 and the $4p_y$, and $4p_z$ orbitals of Br in the *syn*-[8-OO-8BrG]$^{\bullet+}$ product ion, as demonstrated by the molecular orbitals in Figure 2d. Similar conjugation may be expected in the *anti*-[8-OO-8BrG]$^{\bullet+}$ product too. Such conjugate effects, which appear only in the 8BrG$^{\bullet+}$ oxidation products, help attract the reaction system toward the [8-OO-8BrG]$^{\bullet+}$ products; secondly, the CASPT2-calculated activation free energy ($\Delta G^{\ddagger}$) is -0.35 eV for the C8-addition to 8BrG$^{\bullet+}$ vs. -0.21 eV to G$^{\bullet+}$, which renders the reaction of 8BrG$^{\bullet+}$ more kinetically favorable. We had assumed that the enhanced reactivity might also be related to the electron-withdrawing nature of the Br atom. To this end, we performed charge analysis for the TS8c and *syn*-[8-OO-8BrG]$^{\bullet+}$ structures along the most probable reaction pathway, and compared them with the same type of transition state and product in the reaction of G$^{\bullet+}$. It was found that the Br substituent does influence the electron density at

the C8-position, but not to the extent that would significantly promote an electrophilic addition.

4. Conclusions

A gas-phase guided-ion beam scattering study was carried out for the reaction of $^1O_2$ with 8BrGuo$^{\bullet+}$ and its prototype system 8BrG$^{\bullet+}$, augmented by computational explorations of the reaction PES for the model system. The measurement of reaction cross sections and their E_{col} dependence for 8BrG$^{\bullet+}$/8BrGuo$^{\bullet+}$ + $^1O_2$ indicates that both reactions produce exothermic products and have no activation barriers leading to products; more specifically, the exothermicity of the oxidation reaction is sufficiently large that it is enough to eliminate a water ligand in monohydrated peroxide products. Among the various single- and multi-reference levels of theory and approximate spin projection approach utilized in PES calculations, the CASPT2(21,15) theory provided the best description of the reaction as well as a quantitative agreement with the experimental data. The comprehensive theoretical modeling has deemed the C8-peroxide as the kinetically most favorable and thermodynamically most feasible product. Finally, the fact that 8BrG$^{\bullet+}$ has a much higher reactivity toward $^1O_2$ than the unsubstituted G$^{\bullet+}$ has manifested the influence of the 8-Br substituent both in product electronic structure and in reaction kinetics. The results of this work are of particular interest in biological systems as it illustrates the synergistic, oxidatively generated damage of 8BrG$^{\bullet+}$ and 8BrGuo$^{\bullet+}$ that can occur upon one-electron oxidation, ionizing radiation and $^1O_2$ oxidation.

Acknowledgement

This work was supported by National Science Foundation (Grant No. CHE 1856362). J.B. acknowledges the Early Research Initiative Catalyst Grant from the CUNY Graduate Center. T.S. acknowledges the fund for the Promotion of Joint International Research (Fostering Joint International Research (B)) and for the Grants-in-Aid for Scientific Research (C) from the Japan Society for the Promotion of Science (Nos. 18KK0194 and 21K04985).

Supporting Information

8BrG$^{\bullet+}$ tautomers and Cartesian coordinates for calculated structures

References

(1) Thomas, E. L.; Bozeman, P. M.; Jefferson, M. M.; King, C. C., Oxidation of Bromide by the Human Leukocyte Enzymes Myeloperoxidase and Eosinophil Peroxidase. Formation of Bromamines. *J. Biol. Chem.* **1995,** *270*, 2906-2913.

(2) Weiss, S. J.; Test, S. T.; Eckmann, C. M.; Roos, D.; Regiani, S., Brominating Oxidants Generated by Human Eosinophils. *Science* **1986,** *234*, 200-203.

(3) Gaut, J. P.; Yeh, G. C.; Tran, H. D.; Byun, J.; Henderson, J. P.; Richter, G. M.; Brennan, M.-L.; Lusis, A. J.; Belaaouaj, A.; Hotchkiss, R. S., et al., Neutrophils Employ the Myeloperoxidase System to Generate Antimicrobial Brominating and Chlorinating Oxidants During Sepsis. *Proc. Natl. Acad. Sci.* **2001,** *98*, 11961-11966.

(4) Shen, Z.; Mitra, S. N.; Wu, W.; Chen, Y.; Yang, Y.; Qin, J.; Hazen, S. L., Eosinophil Peroxidase Catalyzes Bromination of Free Nucleosides and Double-Stranded DNA. *Biochem.* **2001,** *40*, 2041-2051.

(5) Pattison, D. I.; Davies, M. J., Kinetic Analysis of the Reactions of Hypobromous Acid with Protein Components: Implications for Cellular Damage and Use of 3-Bromotyrosine as a Marker of Oxidative Stress. *Biochem.* **2004,** *43*, 4799-4809.

(6) Henderson, J. P.; Byun, J.; Williams, M. V.; Mueller, D. M.; McCormick, M. L.; Heinecke, J. W., Production of Brominating Intermediates by Myeloperoxidase. A Transhalogenation Pathway for Generating Mutagenic Nucleobases During Inflammation. *J. Biol. Chem.* **2001,** *276*, 7867-7875.

(7) Cadet, J.; Mascio, P. D., 8-Oxo-7,8-Dihydro-2'-Deoxyguanosine: A Major DNA Oxidation Product In *Modified Nucleosides: In Biochemistry, Biotechnology and Medicine*, Herdewijn, P., Ed. Wiley-VCH Verlag Gmbh & Co. KGaA: Weinheim, 2008; pp 29-47.

(8) Asahi, T.; Kondo, H.; Masuda, M.; Nishino, H.; Aratani, Y.; Naito, Y.; Yoshikawa, T.; Hisaka, S.; Kato, Y.; Osawa, T., Chemical and Immunochemical Detection of 8-Halogenated Deoxyguanosines at Early Stage Inflammation. *J. Biol. Chem.* **2010,** *285*, 9282-9291.

(9) Sassa, A.; Ohta, T.; Nohmi, T.; Honma, M.; Yasui, M., Mutational Specificities of Brominated DNA Adducts Catalyzed by Human DNA Polymerases. *J. Mol. Biol.* **2011,** *406*, 679-686.

(10) Koag, M.-C.; Min, K.; Lee, S., Structural Basis for Promutagenicity of 8-Halogenated Guanine. *J. Biol. Chem.* **2014,** *289*, 6289-6298.

(11) Shinmura, K.; Kato, H.; Tao, H.; Inoue, Y.; Nakamura, S.; Yoshida, H.; Tsuzaki, E.; Sugimura, H.; Goto, M., Mutation Spectrum Induced by 8-Bromoguanine, a Base Damaged by Reactive Brominating Species, in Human Cells. *Oxid Med Cell Longev* **2017,** *2017*, 7308501.

(12) Razskazovskii, Y.; Swarts, S. G.; Falcone, J. M.; Taylor, C.; Sevilla, M. D., Competitive Electron Scavenging by Chemically Modified Pyrimidine Bases in Bromine-Doped DNA: Relative Efficiencies and Relevance to Intrastrand Electron Migration Distances. *J. Phys. Chem. B* **1997,** *101*, 1460-1467.

(13) Boussicault, F.; Kaloudis, P.; Caminal, C.; Mulazzani, Q. G.; Chatgilialoglu, C., The Fate of C5' Radicals of Purine Nucleosides under Oxidative Conditions. *J. Am. Chem. Soc.* **2008,** *130*, 8377-8385.

(14) Chatgilialoglu, C.; Caminal, C.; Altieri, A.; Vougioukalakis, G. C.; Mulazzani, Q. G.; Gimisis, T.; Guerra, M., Tautomerism in the Guanyl Radical. *J. Am. Chem. Soc.* **2006,** *128*, 13796-13805.

(15) Fazio, D.; Trindler, C.; Heil, K.; Chatgilialoglu, C.; Carell, T., Investigation of Excess-Electron Transfer in DNA Double-Duplex Systems Allows Estimation of Absolute Excess-Electron Transfer and CPD Cleavage Rates. *Chem. - Eur. J.* **2011,** *17*, 206-212.

(16) Chomicz, L.; Furmanchuk, A. o.; Leszczynski, J.; Rak, J., Electron Induced Single Strand Break and Cyclization: A Dft Study on the Radiosensitization Mechanism of the Nucleotide of 8-Bromoguanine. *Phys. Chem. Chem. Phys.* **2014,** *16*, 6568-6574.

(17) Zhou, J.; Kostko, O.; Nicolas, C.; Tang, X.; Belau, L.; de Vries, M. S.; Ahmed, M., Experimental Observation of Guanine Tautomers with Vuv Photoionization. *J. Phys. Chem. A* **2009,** *113*, 4829-4832.

(18) Schwell, M.; Hochlaf, M., Photoionization Spectroscopy of Nucleobases and Analogues in the Gas Phase Using Synchrotron Radiation as Excitation Light Source. *Top. Curr. Chem.* **2015,** *355*, 155-208.

(19) Touboul, D.; Gaie-Levrel, F.; Garcia, G. A.; Nahon, L.; Poisson, L.; Schwell, M.; Hochlaf, M., Vuv Photoionization of Gas Phase Adenine and Cytosine: A Comparison between Oven and Aerosol Vaporization. *J. Chem. Phys.* **2013,** *138*, 094203.

(20) Jochims, H.-W.; Schwell, M.; Baumgaertel, H.; Leach, S., Photoion Mass Spectrometry of Adenine, Thymine and Uracil in the 6-22 eV Photon Energy Range. *Chem. Phys.* **2005,** *314*, 263-282.

(21) *Singlet Oxygen: Applications in Biosciences and Nanosciences, Volume 1. [In: Compr. Ser. Photochem. Photobiol. Sci., 2016; 13]*. Nonell, S.; Flors, C. Ed.; RSC: Cambridge, 2016; p 472 pp.

(22) *Singlet Oxygen: Applications in Biosciences and Nanosciences, Volume 2. [In: Compr. Ser. Photochem. Photobiol. Sci., 2016; 14]*. Nonell, S.; Flors, C. Ed.; RSC: Cambridge, 2016; p 332 pp.

(23) Di Mascio, P.; Martinez, G. R.; Miyamoto, S.; Ronsein, G. E.; Medeiros, M. H. G.; Cadet, J., Singlet Molecular Oxygen Reactions with Nucleic Acids, Lipids, and Proteins. *Chem. Rev.* **2019,** *119*, 2043-2086.
(24) Sheu, C.; Foote, C. S., Endoperoxide Formation in a Guanosine Derivative. *J. Am. Chem. Soc.* **1993,** *115*, 10446-10447.
(25) Kang, P.; Foote, C. S., Formation of Transient Intermediates in Low-Temperature Photosensitized Oxidation of an 8-^{13}C-Guanosine Derivative. *J. Am. Chem. Soc.* **2002,** *124*, 4865-4873.
(26) Ye, Y.; Muller, J. G.; Luo, W.; Mayne, C. L.; Shallop, A. J.; Jones, R. A.; Burrows, C. J., Formation of ^{13}C-, ^{15}N-, and ^{18}O-Labeled Guanidinohydantoin from Guanosine Oxidation with Singlet Oxygen. Implications for Structure and Mechanism. *J. Am. Chem. Soc.* **2003,** *125*, 13926-13927.
(27) Neeley, W. L.; Essigmann, J. M., Mechanisms of Formation, Genotoxicity, and Mutation of Guanine Oxidation Products. *Chem. Res. Toxicol.* **2006,** *19*, 491-505.
(28) Ravanat, J.-L.; Martinez, G. R.; Medeiros, M. H. G.; Di Mascio, P.; Cadet, J., Singlet Oxygen Oxidation of 2'-Deoxyguanosine. Formation and Mechanistic Insights. *Tetrahedron* **2006,** *62*, 10709-10715.
(29) Gimisis, T.; Cismas, C., Isolation, Characterization, and Independent Synthesis of Guanine Oxidation Products. *Eur. J. Org. Chem.* **2006,** *2006*, 1351-1378.
(30) Cadet, J.; Douki, T.; Ravanat, J.-L., Oxidatively Generated Base Damage to Cellular DNA. *Free Radic. Biol. Med.* **2010,** *49*, 9-21.
(31) Dumont, E.; Gruber, R.; Bignon, E.; Morell, C.; Moreau, Y.; Monari, A.; Ravanat, J.-L., Probing the Reactivity of Singlet Oxygen with Purines. *Nucleic Acids Res.* **2016,** *44*, 56-62.
(32) Dumont, E.; Gruber, R.; Bignon, E.; Morell, C.; Aranda, J.; Ravanat, J.-L.; Tunon, I., Singlet Oxygen Attack on Guanine: Reactivity and Structural Signature within the B-DNA Helix. *Chem. Eur. J.* **2016,** *22*, 12358-12362.
(33) Fleming, A. M.; Burrows, C. J., Formation and Processing of DNA Damage Substrates for the Hneil Enzymes. *Free Radic. Biol. Med.* **2017,** *107*, 35-52.
(34) Thapa, B.; Munk, B. H.; Burrows, C. J.; Schlegel, H. B., Computational Study of Oxidation of Guanine by Singlet Oxygen ($^1\Delta_g$) and Formation of Guanine:Lysine Cross-Links. *Chem. - Eur. J.* **2017,** *23*, 5804-5813.
(35) Lu, W.; Liu, J., Capturing Transient Endoperoxide in the Singlet Oxygen Oxidation of Guanine. *Chem. Eur. J.* **2016,** *22*, 3127-3138.
(36) Lu, W.; Teng, H.; Liu, J., How Protonation and Deprotonation of 9-Methylguanine Alter Its Singlet O_2 Addition Path: About the Initial Stage of Guanine Nucleoside Oxidation. *Phys. Chem. Chem. Phys.* **2016,** *18*, 15223-15234.
(37) Lu, W.; Sun, Y.; Tsai, M.; Zhou, W.; Liu, J., Singlet O_2 Oxidation of Deprotonated Guanine-Cytosine Base Pair and Its Entangling with Intra-Base-Pair Proton Transfer. *ChemPhysChem* **2018,** *19*, 2645-2654.
(38) Lu, W.; Sun, Y.; Zhou, W.; Liu, J., Ph-Dependent Singlet O_2 Oxidation Kinetics of Guanine and 9-Methylguanine: An Online Mass Spectrometry and Spectroscopy Study Combined with Theoretical Exploration. *J. Phys. Chem. B* **2018,** *122*, 40-53.
(39) Sun, Y.; Tsai, M.; Zhou, W.; Lu, W.; Liu, J., Reaction Kinetics, Product Branching, and Potential Energy Surfaces of $^1O_2$-Induced 9-Methylguanine–Lysine Cross-Linking: A Combined Mass Spectrometry, Spectroscopy, and Computational Study. *J. Phys. Chem. B* **2019,** *123*, 10410-10423.
(40) Sun, Y.; Tsai, M.; Moe, M. M.; Liu, J., Dynamics and Multiconfiguration Potential Energy Surface for the Singlet O_2 Reactions with Radical Cations of Guanine, 9-Methylguanine, 2′-Deoxyguanosine, and Guanosine. *J. Phys. Chem. A* **2021,** *125*, 1564-1576.
(41) Moe, M. M.; Tsai, M.; Liu, J., Singlet Oxygen Oxidation of the Radical Cations of 8-Oxo-2′-Deoxyguanosine and Its 9-Methyl Analogue: Dynamics, Potential Energy Surface, and Products Mediated by C5-O_2-Addition. *ChemPlusChem* **2021,** *86*, 1243-1254.
(42) Burrows, C. J.; Muller, J. G., Oxidative Nucleobase Modifications Leading to Strand Scission. *Chem. Rev.* **1998,** *98*, 1109-1151.
(43) Bruner, S. D.; Norman, D. P. G.; Verdine, G. L., Structural Basis for Recognition and Repair of the Endogenous Mutagen 8-Oxoguanine in DNA. *Nature* **2000,** *403*, 859-866.
(44) Marnett, L. J.; Burcham, P. C., Endogenous DNA Adducts: Potential and Paradox. *Chem. Res. Toxicol.* **1993,** *6*, 771-85.
(45) Palumbo, G., Photodynamic Therapy and Cancer: A Brief Sightseeing Tour. *Expert Opin. Drug Delivery* **2007,** *4*, 131-148.
(46) Sheu, C.; Foote, C. S., Photosensitized Oxygenation of a 7,8-Dihydro-8-Oxoguanosine Derivative. Formation of Dioxetane and Hydroperoxide Intermediates. *J. Am. Chem. Soc.* **1995,** *117*, 474-477.
(47) Buchko, G. W.; Wagner, J. R.; Cadet, J.; Raoul, S.; Weinfeld, M., Methylene Blue-Mediated Photooxidation of 7,8-Dihydro-8-Oxo-2'-Deoxyguanosine. *Biochim. Biophys. Acta, Gene Struct. Expression* **1995,** *1263*, 17-24.

(48) Raoul, S.; Cadet, J., Photosensitized Reaction of 8-Oxo-7,8-Dihydro-2'-Deoxyguanosine: Identification of 1-(2-Deoxy-*β*-D-*Erythro*-Pentofuranosyl)Cyanuric Acid as the Major Singlet Oxygen Oxidation Product. *J. Am. Chem. Soc.* **1996,** *118*, 1892-1898.
(49) Hickerson, R. P.; Prat, F.; Muller, J. G.; Foote, C. S.; Burrows, C. J., Sequence and Stacking Dependence of 8-Oxoguanine Oxidation: Comparison of One-Electron Vs Singlet Oxygen Mechanisms. *J. Am. Chem. Soc.* **1999,** *121*, 9423-9428.
(50) Luo, W. M., J. G.; Rachlin, E. M.; Burrows, C. J., Characterization of Spiroiminodihydantoin as a Product of One-Electron Oxidation of 8-Oxo-7,8-Dihydroguanosine. *Org. Lett.* **2000,** *2*, 613-616.
(51) Duarte, V.; Gasparutto, D.; Yamaguchi, L. F.; Ravanat, J.-L.; Martinez, G. R.; Medeiros, M. H. G.; Di Mascio, P., Paolo ; Cadet, J., Oxaluric Acid as the Major Product of Singlet Oxygen-Mediated Oxidation of 8-Oxo-7,8-Dihydroguanine in DNA. *J. Am. Chem. Soc.* **2000,** *122*, 12622-12628.
(52) Duarte, V.; Gasparutto, D.; Jaquinod, M.; Ravanat, J.-L.; Cadet, J., Repair and Mutagenic Potential of Oxaluric Acid, a Major Product of Singlet Oxygen-Mediated Oxidation of 8-Oxo-7,8-Dihydroguanine. *Chem. Res. Toxicol.* **2001,** *14*, 46-53.
(53) Martinez, G. R.; Medeiros, M. H. G.; Ravanat, J.-L.; Cadet, J.; Di Mascio, P., [^{18}O]-Labeled Singlet Oxygen as a Tool for Mechanistic Studies of 8-Oxo-7,8-Dihydroguanine Oxidative Damage: Detection of Spiroiminodihydantoin, Imidazolone and Oxazolone Derivatives. *Biol. Chem.* **2002,** *383*, 607-617.
(54) McCallum, J. E. B.; Kuniyoshi, C. Y.; Foote, C. S., Characterization of 5-Hydroxy-8-Oxo-7,8-Dihydroguanosine in the Photosensitized Oxidation of 8-Oxo-7,8-Dihydroguanosine and Its Rearrangement to Spiroiminodihydantoin. *J. Am. Chem. Soc.* **2004,** *126*, 16777-16782.
(55) Munk, B. H.; Burrows, C. J.; Schlegel, H. B., An Exploration of Mechanisms for the Transformation of 8-Oxoguanine to Guanidinohydantoin and Spiroiminodihydantoin by Density Functional Theory. *J. Am. Chem. Soc.* **2008,** *130*, 5245-5256.
(56) Sun, Y.; Lu, W.; Liu, J., Exploration of the Singlet O_2 Oxidation of 8-Oxoguanine by Guided-Ion Beam Scattering and Density Functional Theory: Changes of Reaction Intermediates, Energetics, and Kinetics Upon Protonation/Deprotonation and Hydration. *J. Phys. Chem. B* **2017,** *121*, 956-966.
(57) Midey, A.; Dotan, I.; Viggiano, A. A., Temperature Dependences for the Reactions of O^- and O_2^- with $O_2(a^1\Delta_g)$ from 200 to 700 K. *J. Phys. Chem. A* **2008,** *112*, 3040-3045.
(58) Fang, Y.; Liu, F.; Bennett, A.; Ara, S.; Liu, J., Experimental and Trajectory Study on Reaction of Protonated Methionine with Electronically Excited Singlet Molecular Oxygen (a^1D_g): Reaction Dynamics and Collision Energy Effects. *J. Phys. Chem. B* **2011,** *115*, 2671-2682.
(59) Liu, F.; Emre, R.; Lu, W.; Liu, J., Oxidation of Gas-Phase Hydrated Protonated/Deprotonated Cysteine: How Many Water Ligands Are Sufficient to Approach Solution-Phase Photooxidation Chemistry? *Phys. Chem. Chem. Phys.* **2013,** *15*, 20496-20509.
(60) Fang, Y.; Liu, J., Reaction of Protonated Tyrosine with Electronically Excited Singlet Molecular Oxygen ($a^1\Delta_g$): An Experimental and Trajectory Study. *J. Phys. Chem. A* **2009,** *113*, 11250-11261.
(61) Chu, I. K.; Rodriquez, C. F.; Lau, T.-C.; Hopkinson, A. C.; Siu, K. W. M., Molecular Radical Cations of Oligopeptides. *J. Phys. Chem. B* **2000,** *104*, 3393-3397.
(62) Feketeová, L.; Yuriev, E.; Orbell, J. D.; Khairallah, G. N.; O'Hair, R. A. J., Gas-Phase Formation and Reactions of Radical Cations of Guanosine, Deoxyguanosine and Their Homodimers and Heterodimers. *Int. J. Mass Spectrom.* **2011,** *304*, 74-82.
(63) Cheng, P.; Bohme, D. K., Gas-Phase Formation of Radical Cations of Monomers and Dimers of Guanosine by Collision-Induced Dissociation of Cu(II)-Guanosine Complexes. *J. Phys. Chem. B* **2007,** *111*, 11075-11082.
(64) Kumar, A.; Sevilla, M. D., Proton Transfer Induced Somo-to-Homo Level Switching in One-Electron Oxidized A-T and G-C Base Pairs: A Density Functional Theory Study. *J. Phys. Chem. B* **2014,** *118*, 5453-5458.
(65) Frisch, M. J.; Trucks, G. W.; Schlegel, H. B.; Scuseria, G. E.; Robb, M. A.; Cheeseman, J. R.; Scalmani, G.; Barone, V.; Petersson, G. A.; Nakatsuji, H., et al. *Gaussian 16 Rev. B.01*, Wallingford, CT, 2016.
(66) Glendening, E. D.; Badenhoop, J. K.; Reed, A. E.; Carpenter, J. E.; Bohmann, J. A.; Morales, C. M.; Landis, C. R.; Weinhold, F. *NBO 6.0*, Theoretical Chemistry Institute, University of Wiscosin: Madison, WI, 2013.
(67) Maranzana, A.; Ghigo, G.; Tonachini, G., Diradical and Peroxirane Pathways in the [Π2 + Π2] Cycloaddition Reactions of $^1\delta_g$ Dioxygen with Ethene, Methyl Vinyl Ether, and Butadiene: A Density Functional and Multireference Perturbation Theory Study. *J. Am. Chem. Soc.* **2000,** *122*, 1414-1423.
(68) Lee, T. J.; Taylor, P. R., A Diagnostic for Determining the Quality of Single-Reference Electron Correlation Methods. *Int. J. Quantum Chem., Quantum Chem. Symp.* **1989,** *36*, 199-207.
(69) Jayatilaka, D.; Lee, T. J., Open-Shell, Coupled-Cluster Theory. *J. Chem. Phys.* **1993,** *98*, 9734-47.

(70) Liakos, D. G.; Sparta, M.; Kesharwani, M. K.; Martin, J. M. L.; Neese, F., Exploring the Accuracy Limits of Local Pair Natural Orbital Coupled-Cluster Theory. *J. Chem. Theory Comput.* **2015,** *11*, 1525-1539.
(71) Neese, F., The Orca Program System. *Wiley Interdiscip. Rev.: Comput. Mol. Sci.* **2012,** *2*, 73-78.
(72) Saito, T.; Nishihara, S.; Kataoka, Y.; Nakanishi, Y.; Matsui, T.; Kitagawa, Y.; Kawakami, T.; Okumura, M.; Yamaguchi, K., Transition State Optimization Based on Approximate Spin-Projection (AP) Method. *Chem. Phys. Lett.* **2009,** *483*, 168-171.
(73) Saito, T.; Nishihara, S.; Kataoka, Y.; Nakanishi, Y.; Kitagawa, Y.; Kawakami, T.; Yamanaka, S.; Okumura, M.; Yamaguchi, K., Reinvestigation of the Reaction of Ethylene and Singlet Oxygen by the Approximate Spin Projection Method. Comparison with Multireference Coupled-Cluster Calculations. *J. Phys. Chem. A* **2010,** *114*, 7967-7974.
(74) Saito, T.; Takano, Y., Spin-Projected Qm/Mm Free Energy Simulations for Oxidation Reaction of Guanine in B−DNA by Singlet Oxygen. *ChemPhysChem* **2021,** *22*, 561-568.
(75) Yamaguchi, K.; Jensen, F.; Dorigo, A.; Houk, K. N., A Spin-Correction Procedure for Unrestricted Hartree-Fock and Moeller-Plesset Wave Functions for Singlet Diradicals and Polyradicals. *Chem. Phys. Lett.* **1988,** *149*, 537-42.
(76) Andersson, K.; Malmqvist, P. A.; Roos, B. O., Second-Order Perturbation Theory with a Complete Active Space Self-Consistent Field Reference Function. *J. Chem. Phys.* **1992,** *96*, 1218-26.
(77) Abe, M.; Gopakmar, G.; Nakajima, T.; Hirao, K., Relativistic Multireference Perturbation Theory: Complete Active-Space Second-Order Perturbation Theory (CASPT2) with the Four-Component Dirac Hamiltonian. In *Radiation Induced Molecular Phenomena in Nucleic Acids*, Shukla, K.; K., M.; Leszczynski, J., Eds. Springer: Netherlands, 2008; pp 157-177.
(78) Roos, B. O.; Taylor, P. R.; Siegbahn, E. M., A Complete Active Space Scf Method (CASSCF) Using a Density Matrix Formulated Super-Ci Approach. *Chem. Phys.* **1980,** *48*, 157-73.
(79) Alecu, I. M.; Zheng, J.; Zhao, Y.; Truhlar, D. G., Computational Thermochemistry: Scale Factor Databases and Scale Factors for Vibrational Frequencies Obtained from Electronic Model Chemistries. *J. Chem. Theory Comput.* **2010,** *6*, 2872-2887.
(80) Fdez. Galván, I.; Vacher, M.; Alavi, A.; Angeli, C.; Aquilante, F.; Autschbach, J.; Bao, J. J.; Bokarev, S. I.; Bogdanov, N. A.; Carlson, R. K., et al., Openmolcas: From Source Code to Insight. *J. Chem. Theory Comput.* **2019,** *15*, 5925-5964.
(81) Aquilante, F.; Autschbach, J.; Baiardi, A.; Battaglia, S.; Borin, V. A.; Chibotaru, L. F.; Conti, I.; Vico, L. D.; Delcey, M.; Galván, I. F., et al., Modern Quantum Chemistry with [Open]Molcas. *J. Chem. Phys.* **2020,** *152*, 214117.
(82) Roca-Sanjuán, D.; Rubio, M.; Merchán, M.; Serrano-Andrés, L., Ab Initio Determination of the Ionization Potentials of DNA and Rna Nucleobases. *J. Chem. Phys.* **2006,** *125*, 084302.
(83) Mishra, S. K.; Mishra, P. C., An Ab Initio Study of Electronic Structure and Spectra of 8-Bromoguanine: A Comparative Study with Guanine. *Spectrochim. Acta, Part A* **2001,** *57A*, 2433-2450.
(84) Troe, J., Statistical Adiabatic Channel Model of Ion-Neutral Dipole Capture Rate Constants. *Chem. Phys. Lett.* **1985,** *122*, 425-430.
(85) Olsen, J.; Roos, B. O.; Jøgensen, P.; Jensen, H. J. A., Determinant Based Configuration Interaction Algorithms for Complete and Restricted Configuration Interaction Spaces. *J. Chem. Phys.* **1988,** *89*, 2185-92.
(86) Sevin, F.; McKee, M. L., Reactions of 1,3-Cyclohexadiene with Singlet Oxygen. A Theoretical Study. *J. Am. Chem. Soc.* **2001,** *123*, 4591-4600.
(87) Marchetti, B.; Karsili, T. N. V., An Exploration of the Reactivity of Singlet Oxygen with Biomolecular Constituents. *Chem. Commun.* **2016,** *52*, 10996-10999.

Table 1. Relative enthalpies (eV, 298 K) calculated at the DFT, CCSD(T) and CASPT2 levels of theory, and the $<S^2>$ and T1 diagnostics of wave functions

Species	Reaction energies (eV)				$<S^2>$ and T1 diagnostics			
	ωB97XD/6-31+G(d,p)		DLPNO-CCSD(T)/ aug-cc-pVTZ [a]	CASPT2/ 6-31G** [a]	$<S^2>$ at ωB97XD		DLPNO-CCSD(T)	
	restricted	spin projected			before [b]	after [c]	$<S^2>$	T1
$8BrG^+$	0.0	0.0	0.0	0.0	0.7663	0.7502	0.75185	0.017557
$^1O_2$					(1.0039)	(0.0314)	0	0.014569
precursor	-1.79	-0.58	-0.57	-1.22	1.7524	0.8335	0.86155	0.025742
C5, C8-cycloaddition								
TS58	0.37	1.02	0.54	0.77	0.7689	0.7501	0.75055	0.023977
$[5,8\text{-OO-8BrG}]^{\cdot+}$	-0.30	0.35	-0.29	0.19	0.7553	0.7500	0.75022	0.0151281
C8-terminal addition								
TS8a	-0.86	-0.20	-0.64	-0.68	0.8748	0.7520	0.75230	0.0185131
TS8b	-0.98	-0.33	-0.86	-0.55	0.7539	0.7500	0.75020	0.0174640
TS8c	-1.06	-0.40	-0.92	-0.84	0.8044	0.7506	0.75182	0.0188697
TS8d	0.51	1.16	0.52	0.69	0.8250	0.7507	0.75043	0.0217877
syn-$[8\text{-OO-8Br-G}]^{\cdot+}$	-1.17	-0.51	-1.08	-0.79	0.7540	0.7500	0.75021	0.0178268
anti-$[8\text{-OO-8Br-G}]^{\cdot+}$	-1.14	-0.48	-1.03	-0.75	0.7539	0.7500	0.75021	0.0178870
C4-terminal addition								
TS4a	-0.39	0.26	-0.15	0.06	0.7614	0.7501	0.75039	0.0191308
TS4b	-0.31	0.35	-0.14	0.19	0.7544	0.7500	0.75022	0.0182988
TS4c	-0.40	0.26	-0.19	0.26	0.7580	0.7500	0.75031	0.0189465
TS4d	0.04	0.70	0.24	0.60	0.7570	0.7500	0.75052	0.0199381
syn-$[4\text{-OO-8Br-G}]^{\cdot+}$	-0.37	0.28	-0.21	0.11	0.7544	0.7500	0.75022	0.0184379
anti-$[4\text{-OO-8Br-G}]^{\cdot+}$	-0.37	0.29	-0.16	0.11	0.7552	0.7500	0.75023	0.0184753
C5-terminal addition								
TS5a	-1.01	-0.35	-0.85	-0.75	0.8631	0.7517	0.75258	0.0183593
TS5b	-1.04	-0.38	-0.88	-0.52	0.7545	0.7500	0.75022	0.0182072
TS5c	-1.06	-0.40	-0.88	-0.51	0.7887	0.7504	0.75130	0.0184958
syn-$[5\text{-OO-8Br-G}]^{\cdot+}$	-1.11	-0.45	-0.95	-0.50	0.7544	0.7500	0.75022	0.0182176
anti-$[5\text{-OO-8Br-G}]^{\cdot+}$	-1.12	-0.46	-0.95	-0.73	0.7549	0.7500	0.75024	0.0185048

[a] using ωB97XD/6-31+G(d,p)-optimized geometries

[b, c] before and after the annihilation of spin contamination. Values in parentheses were obtained by BS-uωB97XD calculations.

Scheme 1 The lowest-energy structures of $8BrG^{\bullet+}$ and $8BrGuo^{\bullet+}$ optimized at the ωB97XD/6-31+G(d,p) level of theory, with atomic numbering schemes. Spin densities are represented by contour plots and NBO charge densities are indicated in numbers. Their Cartesian coordinates are available in the Supporting Information.

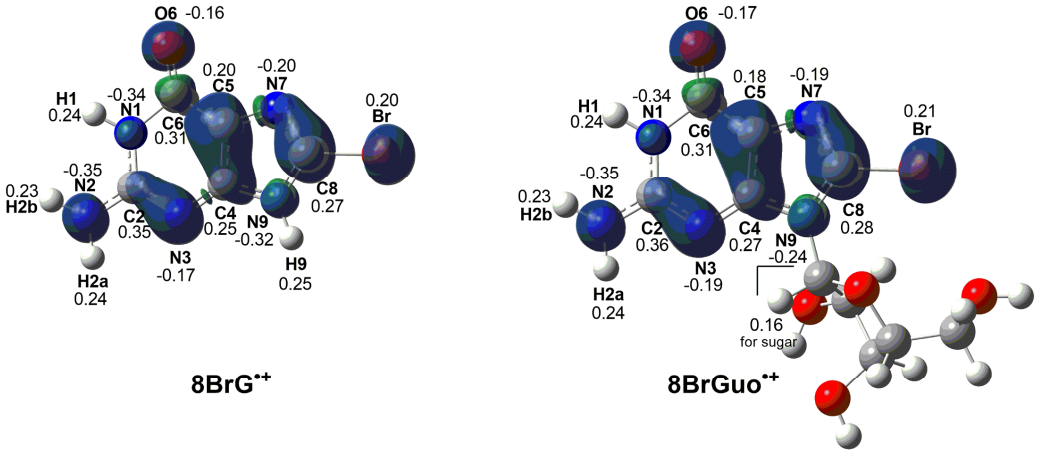

Scheme 2 Structures, hydration energies and relative populations of 8BrG$^{\bullet+}$·H_2O, and the oxidation products of the most stable monohydrate. All were calculated at the ωB97XD/6-31+G(d,p) level of theory. Their Cartesian coordinates are available in the Supporting Information.

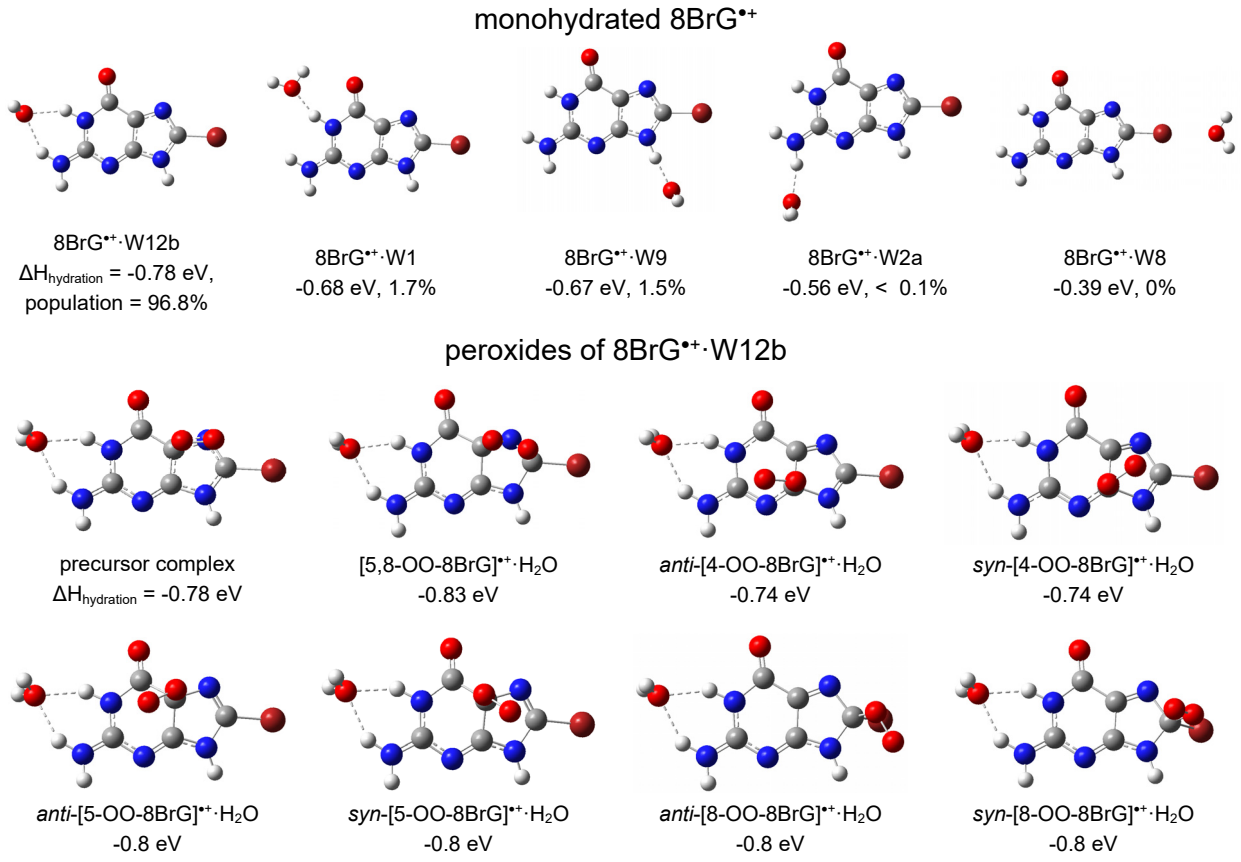

Scheme 3 Reaction pathways for the $^1O_2$ addition to 8BrG$^{\bullet+}$. Cartesian coordinates for these structures are available in the Supporting Information.

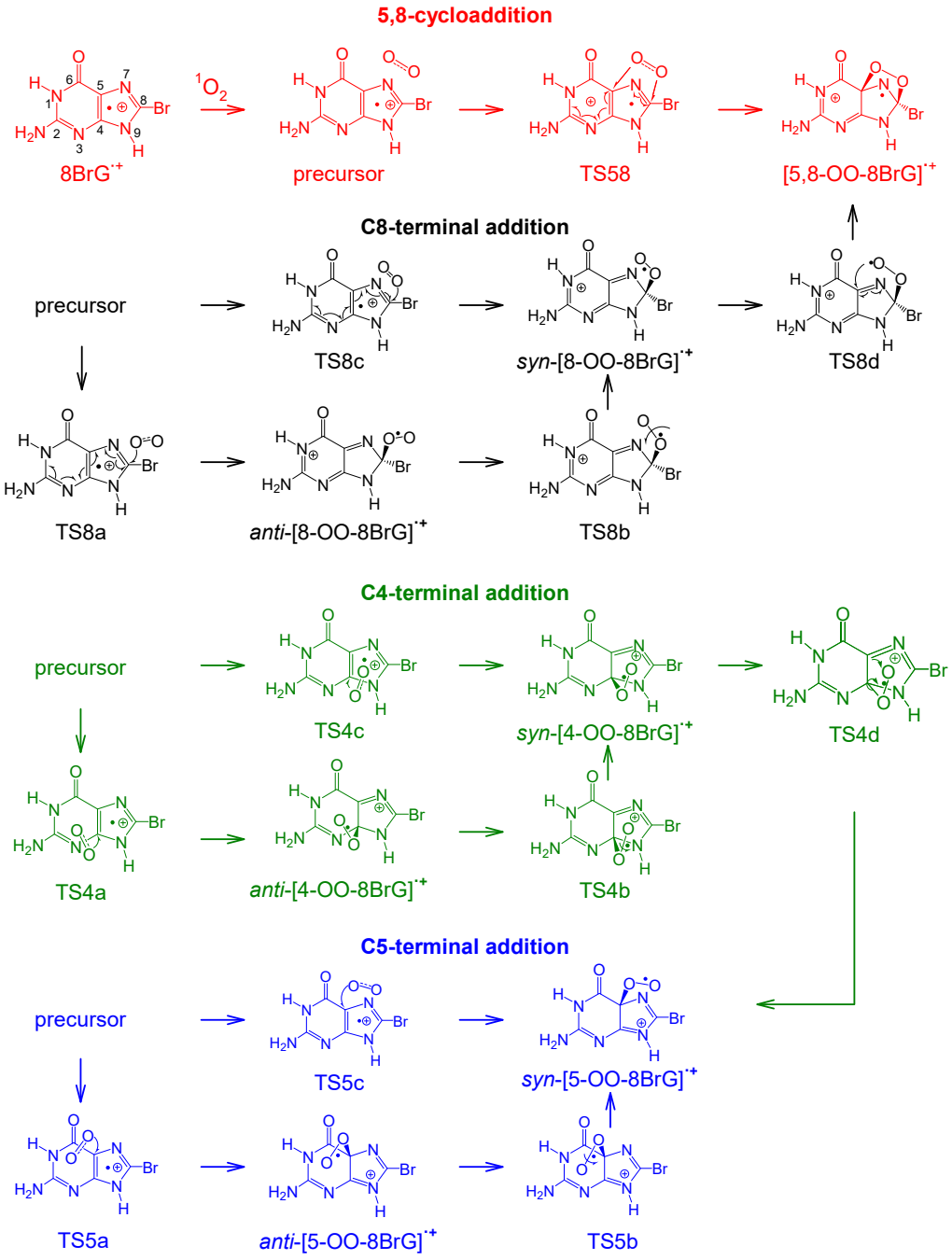

Scheme 4 Spin distributions for the different electronic states of the precursor complex, wherein the numbers indicate NBO spin densities.

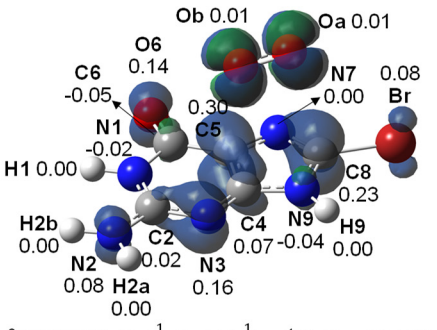

^{2}[8BrG$^{\bullet+}$ (↑, S = $\frac{1}{2}$, m_S = + $\frac{1}{2}$) •••$^{1}O_2$ (↑↓ , S = 0)]

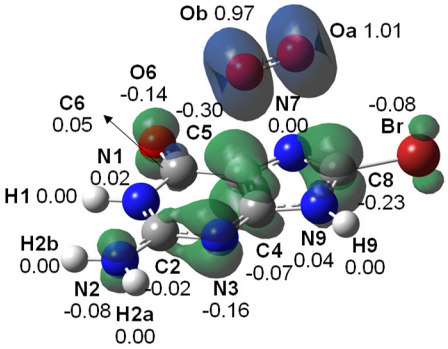

^{2}[8BrG$^{\bullet+}$ (↓ , S = $\frac{1}{2}$, m_S = - $\frac{1}{2}$) •••$^{3}O_2$ (↑↑, S = 1)]

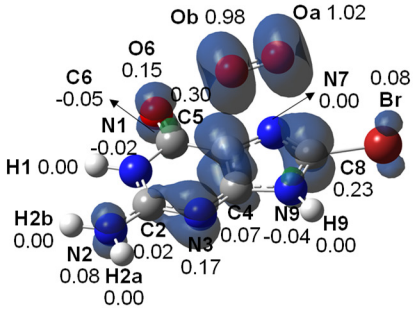

^{4}[8BrG$^{\bullet+}$ (↑, S = $\frac{1}{2}$, m_S = + $\frac{1}{2}$) •••$^{3}O_2$ (↑↑, S = 1)]

Figure Caption

Fig. 1 Product cross sections for the $^1O_2$ reactions with (a) $8BrG^{\bullet+}\cdot H_2O$ and (d) $8BrGuo^{\bullet+}$. Insets show product ion mass spectra, wherein scale factors for the peak intensities of product ions are indicated.

Fig. 2 (a – c) Reaction PES for the $^1O_2$ addition to $8BrG^{\bullet+}$ calculated at different levels of theory, and (d) the conjugation interactions between $\pi(O_2)$ orbitals and $4p_x/4p_y$(Br) orbitals.

Fig. 1

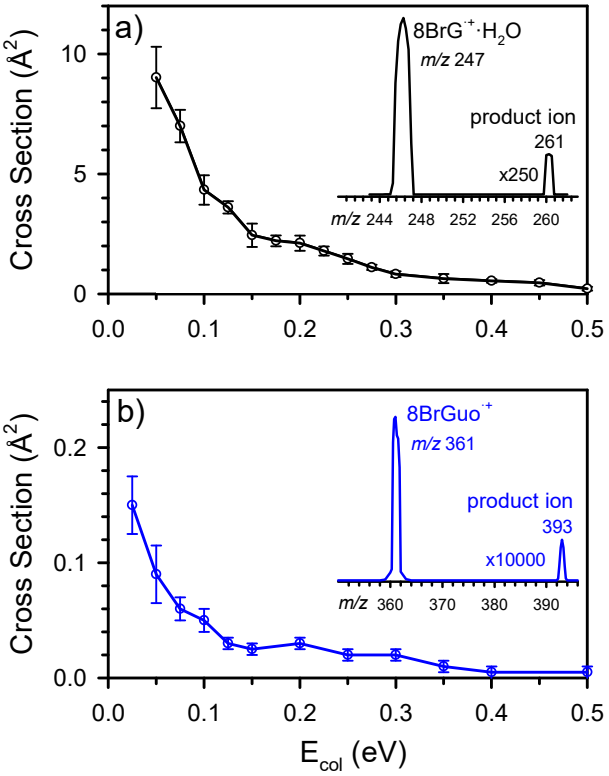
a)
8BrG^{+}·H$_2$O
m/z 247
product ion
261
x250
m/z 244 248 252 256 260
Cross Section (Å^2)
10
5
0
0.0 0.1 0.2 0.3 0.4 0.5
b)
8BrGuo^{+}
m/z 361
product ion
393
x10000
m/z 360 370 380 390
Cross Section (Å^2)
0.2
0.1
0.0
0.0 0.1 0.2 0.3 0.4 0.5
E$_{col}$ (eV)

Fig. 2

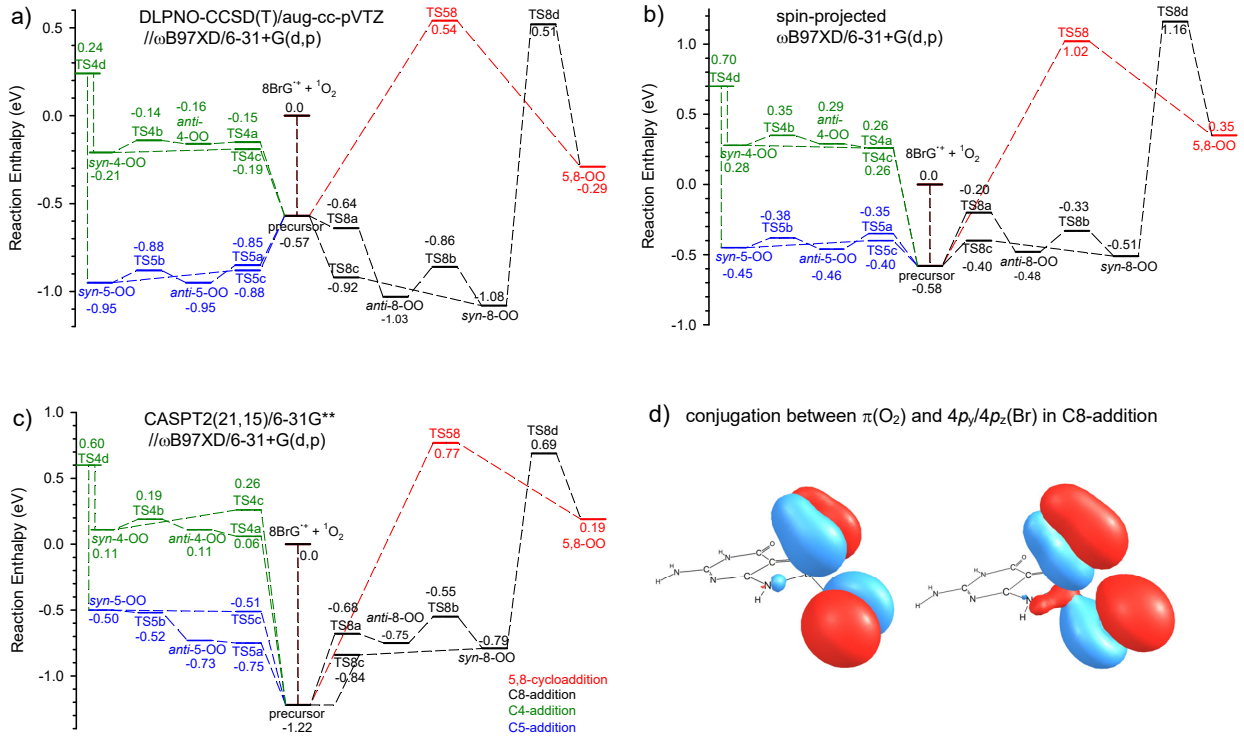
a)
DLPNO-CCSD(T)/aug-cc-pVTZ
//ωB97XD/6-31+G(d,p)
Reaction Enthalpy (eV)
8BrG•+ + 1O2
0.0
TS4d
0.24
TS4b
-0.14
anti-4-OO
-0.16
TS4a
-0.15
TS4c
-0.19
syn-4-OO
-0.21
TS5b
-0.88
TS5a
-0.85
TS5c
-0.88
syn-5-OO
-0.95
anti-5-OO
-0.95
precursor
-0.57
TS8a
-0.64
TS8c
-0.92
TS8b
-0.86
anti-8-OO
-1.03
syn-8-OO
-1.08
TS58
0.54
TS8d
0.51
5,8-OO
-0.29
b)
spin-projected
ωB97XD/6-31+G(d,p)
Reaction Enthalpy (eV)
8BrG•+ + 1O2
0.0
TS4d
0.70
TS4b
0.35
anti-4-OO
0.29
TS4a
0.26
TS4c
0.26
syn-4-OO
0.28
TS5b
-0.38
TS5a
-0.35
TS5c
-0.40
syn-5-OO
-0.45
anti-5-OO
-0.46
precursor
-0.58
TS8a
-0.20
TS8c
-0.40
TS8b
-0.33
anti-8-OO
-0.48
syn-8-OO
-0.51
TS58
1.02
TS8d
1.16
0.35
5,8-OO
c)
CASPT2(21,15)/6-31G**
//ωB97XD/6-31+G(d,p)
Reaction Enthalpy (eV)
8BrG•+ + 1O2
0.0
TS4d
0.60
TS4b
0.19
TS4c
0.26
TS4a
0.06
syn-4-OO
0.11
anti-4-OO
0.11
TS5b
-0.50
TS5c
-0.51
TS5a
-0.75
syn-5-OO
-0.50
anti-5-OO
-0.73
precursor
-1.22
TS8a
-0.68
TS8c
-0.84
TS8b
-0.55
anti-8-OO
-0.75
syn-8-OO
-0.79
TS58
0.77
TS8d
0.69
0.19
5,8-OO
5,8-cycloaddition
C8-addition
C4-addition
C5-addition
d) conjugation between π(O2) and 4py/4pz(Br) in C8-addition

TOC